axioms

MDPI

Article

Swirling Flow of Chemically Reactive Viscoelastic Oldroyd-B Fluid through Porous Medium with a Convected Boundary Condition Featuring the Thermophoresis Particle Deposition and Soret–Dufour Effects

Abeer Al Elaiw [1,*], Abdul Hafeez [2,3], Asma Khalid [1,4] and Muneerah AL Nuwairan [1]

[1] Department of Mathematics and Statistics, College of Science, King Faisal University, P.O. Box 400, Al Ahsa 31082, Saudi Arabia
[2] Department of Mathematics, University of Loralai, Loralai 84800, Pakistan
[3] Department of Mathematics, Quaid-i-Azam University, Islamabad 44000, Pakistan
[4] Department of Mathematics, SBK Women's University, Quetta 87300, Pakistan
* Correspondence: aalelaiw@kfu.edu.sa

Abstract: In this study, an analysis of the rotating flow of viscoelastic Oldroyd-B fluid along with porous medium featuring the Soret–Dufour effects is explored. The heat transport mechanism is discussed with the involvement of thermal radiation and heat source/sink. Additionally, the thermophoresis of particle deposition and chemical reaction are taken into the concentration equation in order to investigate the mass transportation in the liquid. To formulate the non-linear ordinary differential equations, the von Karman similarity approach is used in the system of partial differential equations and then integrated numerically by the bvp midrich scheme in Maple programming. Results are provided by graphical framework and tabular form. A quick parametric survey is carried out concerning flow field, thermal, and solutal distributions through graph representation. The curves show that increasing the values of the retardation time parameter decreases the radial velocity while increasing the angular velocity. Additionally, when the relaxation time parameter becomes powerful, the magnitude of the velocity curves decreases considerably in the radial and axial directions. The presence of a radiation parameter indicates that the fluid will absorb a greater amount of heat, which is equivalent to a higher temperature. Further, an increase in the stretching parameter leads to a reduction in the temperature components.

Keywords: viscoelastic fluid; magnetic field; porous medium; thermophoresis; Soret–Dufour effects; numerical solution

MSC: 00A69; 76A10

check for updates

Citation: Al Elaiw, A.; Hafeez, A.; Khalid, A.; AL Nuwairan, M. Swirling Flow of Chemically Reactive Viscoelastic Oldroyd-B Fluid through Porous Medium with a Convected Boundary Condition Featuring the Thermophoresis Particle Deposition and Soret–Dufour Effects. *Axioms* **2022**, *11*, 608. https://doi.org/10.3390/axioms11110608

Academic Editor: Igor V. Miroshnichenko

Received: 2 October 2022
Accepted: 28 October 2022
Published: 1 November 2022

1. Introduction

In the field of fluid dynamics, research into rotating disk geometry has attracted a great deal of attention and enthusiasm in recent years due to its many potential technical and industrial applications, including jet engines, hard disks, turbine systems, etc. It is for this reason that the phenomenon of fluid flow by a rotating disk has received a significant amount of attention and has been extensively analyzed by researchers, particularly after von Kerman's seminal work on flow by a rotating disk. The overarching goal of the discussion is to study the convection fluid motion of the Oldroyd-B fluid model [1] due to a porous rotating disk using the novel perspective of thermophoresis particle deposition together with the occurrence of Soret–Dufour impacts and chemical reactions.

Von Kármán [2], in his groundbreaking work, simplified the complete set of equations guiding the solution to the rotating disk problem. After that, Cochran [3] made an attempt to numerically solve the Kármán swirling flow problem. Further, Millsaps and Pohlhausen [4] studied the heat transfer properties to accommodate the supplementary extension. For a viscous fluid, Shevchuk and Buschmann [5] found an exact solution to the heat transfer problem in a rotating disk flow. Awad [6] offered the asymptotic solutions to the heat transport properties for a range of Prandtl numbers. Through the use of a rotating porous disc, Turkyilmazoglu [7] was able to obtain the closed-form solution for an incompressible and viscous fluid. In a separate work, Turkyilmazoglu [8] investigated the impacts of radial electric fields on MHD fluid flow and heat transfer for the rotating disk problem. Recently, the study of viscoelastic fluid flow, along with heat transfer, is discussed by Nuwairan et al. [9]. They demonstrated that heat generation/absorption and thermal radiation contribute to raising the liquid's temperature.

The rheological properties of non-Newtonian fluids are very dissimilar to those of Newtonian fluids. Therefore, many different constitutive equations have been developed to describe these fluids. Of these, a great deal of focus has been placed on rate-type models. As earlier, Oldroyd [10] established a methodical approach to creating models of rate-type viscoelastic fluids. He took great effort to incorporate into his framework the invariance requirements that the model ought to be able to fulfill, but there is no indication that the thermodynamical issue has been taken into account. In 2000, Rajagopal and Srinivasa [11] made a systematic thermodynamic framework within which models of a variety of rate-type viscoelastic fluids can be derived. Notable among these is the Oldroyd-B model, which can adequately describe the behavior of some polymeric liquids. Both theoretical and practical testing of this model is feasible. For this reason, many articles related to these fluids have already been published via Refs. [12–15].

A survey of the research available shows that, despite the importance of fluid motion over a porous rotating disk to many different types of industries, researchers have paid it relatively little attention. Thus, the main purpose of this research is to examine the flow of Oldroyd-B fluids due to a rotating disk subject to a convection boundary condition, incorporating thermophoresis and Soret–Dufour impacts. In addition, the study elucidates the significance of heat source/sink and thermal radiation, along with the chemical reaction on the heat and mass transport characteristics that occur during fluid motion. The modeled flow problem is solved numerically by a BVP (boundary value problem) midrich scheme in Maple programming. To highlight the impact of active parameters, tabular and graphical trends are obtained and elaborated in detail.

2. Problem Description

We assume an incompressible magnetized Oldroyd-B fluid flow through porous medium caused by a rotating disk that stretches and rotates at different rates. The surface is considered to be porous, with a mass flux velocity of w_0 ($w_0 < 0$ for suction and $w_0 > 0$ for injection). To express the mathematical modelling of the problem, cylindrical coordinates (r, φ, z) are used. The stretching and rotating velocities of the disk (positioned at $z = 0$) are, respectively, a and Ω, as referred in Figure 1. All physical quantities are not depending on φ, as the flow is axisymmetric in the z direction. By ignoring the induced electric and magnetic fields, a uniform beam of magnetic field, B_0, is imposed along the z-axis. The temperature equation is used along with the presence of heat source/sink and radiation to express the heat transportation in the liquid. For the mass transportation, the chemical reaction and thermophoresis particle deposition are both taken into the concentration equation. Additionally, the impact of Soret and Dufour and the convective boundary condition are also considered.

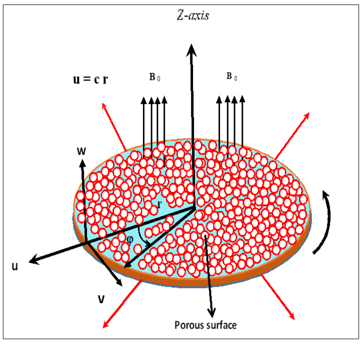

Figure 1. Flow diagram [13].

From the aforementioned assumptions, the modeled equations [1] are as follows:

$$\begin{gathered}\frac{\partial u}{\partial r}+\frac{u}{r}+\frac{\partial w}{\partial z}=0,\\ u\frac{\partial u}{\partial r}-\frac{v^2}{r}+w\frac{\partial u}{\partial z}=\nu\frac{\partial^2 u}{\partial z^2}-\frac{\sigma}{\rho}{B_0}^2\left[u+\lambda_1 w\frac{\partial u}{\partial z}\right]-\frac{\phi_1\nu}{K}u\\ -\lambda_1\left[u^2\frac{\partial^2 u}{\partial r^2}+w^2\frac{\partial^2 u}{\partial z^2}+2uw\frac{\partial^2 u}{\partial r\partial z}-\frac{2vw}{r}\frac{\partial v}{\partial z}+\frac{v^2}{r}\frac{\partial u}{\partial r}-\frac{2uv}{r}\frac{\partial v}{\partial r}+\frac{uv^2}{r^2}\right]\end{gathered}\tag{1}$$

$$\begin{gathered}-\nu\lambda_2\left[-\frac{\partial u}{\partial r}\frac{\partial^2 u}{\partial z^2}-2\frac{\partial u}{\partial z}\frac{\partial^2 w}{\partial z^2}+\frac{\partial^3 u}{\partial z^3}+u\frac{\partial^3 u}{\partial r\partial z^2}-\frac{1}{r}\left(\frac{\partial u}{\partial z}\right)^2-\frac{\partial u}{\partial z}\frac{\partial^2 u}{\partial r\partial z}\right],\\ u\frac{\partial v}{\partial r}+\frac{uv}{r}+w\frac{\partial v}{\partial z}=\nu\frac{\partial^2 v}{\partial z^2}-\frac{\sigma}{\rho}{B_0}^2\left[v+\lambda_1 w\frac{\partial v}{\partial z}\right]-\frac{\phi_1\nu}{K}v\\ -\lambda_1\left[u^2\frac{\partial^2 v}{\partial r^2}+\frac{2uv}{r}\frac{\partial u}{\partial r}+w^2\frac{\partial^2 v}{\partial z^2}+\frac{2vw}{r}\frac{\partial u}{\partial z}+2uw\frac{\partial^2 v}{\partial r\partial z}+\frac{v^2}{r}\frac{\partial v}{\partial r}-2\frac{u^2 v}{r^2}--\frac{v^3}{r^2}\right]\end{gathered}\tag{2}$$

$$-\nu\lambda_2\left[-\frac{\partial v}{\partial r}\frac{\partial^2 u}{\partial z^2}+u\frac{\partial^3 v}{\partial r\partial z^2}-\frac{\partial v}{\partial z}\frac{\partial^2 u}{\partial r\partial z}-\frac{1}{r}\frac{\partial u}{\partial z}\frac{\partial v}{\partial z}-2\frac{\partial v}{\partial z}\frac{\partial^2 w}{\partial z^2}+\frac{v}{r}\frac{\partial^2 u}{\partial z^2}+w\frac{\partial^3 u}{\partial z^3}-\frac{u}{r}\frac{\partial^2 v}{\partial z^2}\right],\tag{3}$$

$$u\frac{\partial T}{\partial r}+w\frac{\partial T}{\partial z}=\frac{k_1^*}{\rho c_p}\left(\frac{\partial^2 T}{\partial z^2}\right)-\frac{1}{\rho c_p}\frac{\partial q_{rad}}{\partial z}+\frac{Dk_T}{c_s c_p}\frac{\partial^2 C}{\partial z^2}+\frac{Q_0}{\rho c_p}(T-T_\infty),\tag{4}$$

$$u\frac{\partial C}{\partial r}+w\frac{\partial C}{\partial z}=D_m\frac{\partial^2 C}{\partial z^2}+\frac{D_m k_T}{T_m}\frac{\partial^2 T}{\partial z^2}-K_1 C-\frac{\partial(U_T C)}{\partial r}-\frac{\partial(W_T C)}{\partial z},\tag{5}$$

The radiative flux q_{rad} [13,16] is given by:

$$q_{rad}=-\frac{4}{3}\frac{\sigma^*}{k^*}\frac{\partial T^4}{\partial z},\tag{6}$$

The thermophoretic velocities are defined by:

$$U_T=-k\nu\frac{1}{T}\frac{\partial T}{\partial r}\text{ and }W_T=-k\nu\frac{1}{T}\frac{\partial T}{\partial z},\tag{7}$$

where the values of k are in the range of 0.2 to 1.2, as expressed by Batchelor and Shen [17], and are defined from the theory of Talbot et al. [18] by:

$$\frac{2C_s\left(\lambda_g/\lambda_p+C_t Kn\right)\left[1+Kn\left(C_1+C_2 e^{-C_3/kn}\right)\right]}{(1+3C_m Kn)\left[1+\lambda_g/\lambda_p+2C_t Kn\right]}\tag{8}$$

where $(C_s,\ C_t, C_m, C_1, C_2,\ C_3)=(1.147,\ 2.20,\ 1.146,\ 1.2,\ 0.41,\ 0.88)$ are, respectively, constants. Additionally, Kn is the Knudsen number and (λ_p, λ_g) are the thermal conductivities of the diffusion particles and the fluid. The respective boundary conditions are:

$$\begin{gathered}u=cr, v=\Omega\mathrm{r},\ \mathrm{w}=w_0, -k_1^*\frac{\partial T}{\partial z}=h_f\left(T_f-T\right), C=C_w\text{ at }z=0,\\ u\to 0, v\to 0, T\to T_\infty, C\to C_\infty\text{ as }z\to\infty\end{gathered}\tag{9}$$

Introducing the similarity variables [13] are:

$$\begin{aligned}(\eta, u, v, w) &= \left(\sqrt{\frac{\Omega}{\nu}}z,\ \Omega rF,\ \Omega rG,\ \sqrt{\Omega\nu}H\right),\\ [T, C, \Delta T] &= \left[T_\infty + \Delta T\theta,\ C_\infty\phi,\ T_f - T_\infty\right]\end{aligned} \tag{10}$$

Applying Equation (10) into Equations (1)–(5), we have:

$$H' + 2F = 0, \tag{11}$$

$$\begin{gathered}F^2 - G^2 + F'H - F'' + \gamma F + \beta_1\left(F''H^2 + 2FF'H - 2GG'H\right) + \beta_2\left(2F'^2 + 2F'H'' - F'''H\right)\\ +M(F + \beta_1 F'H) = 0,\end{gathered} \tag{12}$$

$$\begin{gathered}2FG - G'' + G'H + \gamma G + \beta_1\left(G''H^2 + 2(F'G + FG')H\right) - \beta_2(-2F'G' + G'''H - 2G'H'')\\ +M(\beta_1 G'H + G) = 0,\end{gathered} \tag{13}$$

$$\theta'' + \frac{4}{3}\mathrm{Rd}\theta'' - \mathrm{Pr}H\theta' + \mathrm{Pr}\ Du\ \phi'' + \mathrm{Pr}\ \delta\ \theta = 0, \tag{14}$$

$$\frac{1}{\mathrm{Sc}}\phi'' - H\phi' - K_r\phi + \mathrm{Sr}\theta'' + \frac{k\mathrm{Nt}}{(1 + \mathrm{Nt}\theta)}\theta''\phi - \frac{k(\mathrm{Nt})^2}{(1 + \mathrm{Nt}\theta)^2}\theta'^2\phi + \frac{k\mathrm{Nt}}{(1 + \mathrm{Nt}\theta)}\theta'\phi' = 0. \tag{15}$$

The transformed boundary conditions (BCs) are:

$$\begin{gathered}F(\eta) = R, G(\eta) = 1, H(\eta) = s, \theta'(\eta) = -\mathrm{Bi}(1 - \theta(\eta)), \phi(\eta) = 0 \text{ at } \eta = 0,\\ F(\eta) \to 0, G(\eta) \to 0, \theta(\eta) \to 0, \phi(\eta) \to 1 \text{ as } \eta \to \infty,\end{gathered} \tag{16}$$

The parameters are expressed as:

$$\begin{gathered}M = \left(\frac{\sigma B_0^2}{\rho\Omega}\right), R = \left(\frac{c}{\Omega}\right), \beta_1 = (\lambda_1\Omega), \gamma = \left(\frac{\nu\phi_1}{\Omega K}\right), s = \left(\frac{w_0}{\sqrt{\Omega\nu}}\right), \mathrm{Rd} = \left(\frac{4}{3}\frac{\sigma^* T_\infty^3}{k_1^* k^*}\right),\ \mathrm{Bi} = \left(\frac{h_f\sqrt{\frac{\nu}{\Omega}}}{k_1^*}\right),\\ \delta = \left(\frac{Q_0}{\Omega\rho c_p}\right), \beta_2 = (\lambda_2\Omega), K_r = \left(\frac{K_1}{\Omega}\right), \mathrm{Du} = \left(\frac{D_m k_T}{c_s c_p \nu}\frac{C_\infty}{\Delta \mathrm{T}}\right),\ \mathrm{Sr} = \left(\frac{D_m k_T}{T_m \nu}\frac{\Delta \mathrm{T}}{C_\infty}\right),\ \mathrm{Pr} = \left(\frac{\nu(\rho c_p)}{k_1^*}\right),\\ \mathrm{Sc} = \left(\frac{\nu}{D_m}\right) \text{ and } \mathrm{Nt} = \left(\frac{\Delta \mathrm{T}}{T_\infty}\right)\end{gathered} \tag{17}$$

The physical parameters are defined as:
The Nusselt number, $\mathrm{Nu_r}$, and Sherwood number, $\mathrm{Sh_r}$, are of the form:

$$\mathrm{Nu_r} = -\frac{rk_1^*\left(\left[\frac{\partial T}{\partial z}\right] + q_{rad}\right)_{z=0}}{k_1^*\left(T_f - T_\infty\right)},\ \text{and}\ \mathrm{Sh_r} = \frac{rD_m\left(\frac{\partial C}{\partial z}\right)_{z=0}}{D_m(C_w - C_\infty)} \tag{18}$$

Their dimensionless forms are:

$$\mathrm{Re}^{-\frac{1}{2}}\ \mathrm{Nu_r} = -\left\{1 + \frac{4\mathrm{Rd}}{3}\right\}\theta'(0),\ \text{and}\ \mathrm{Re}^{-\frac{1}{2}}\ \mathrm{Sh_r} = -\phi'(0), \tag{19}$$

in which, $\mathrm{Re} = \left(\frac{r^2\Omega}{\nu}\right)$ is the local Reynold number.

3. Results and Discussion

In this section, a discussion is presented in the form of graphs and tables regarding the effect different physical parameters have had on the current investigation. These results are achieved through the utilization of the numerical technique called the bvp midrich Maple package. In light of this, the following fixed values are assigned for the computations: $M = 2.0$, $\beta = 0.05$, $R = 1.3$, $s = 0.1$, $\mathrm{Pr} = 6.5$, $\mathrm{Sc} = 6.5$, $\mathrm{Sr} = 0.1$, $K_2 = 0.01$, $\mathrm{Du} = 0.1$, $\gamma = 0.1$, $\mathrm{Rd} = 0.1$, $\mathrm{Bi} = 0.1$, $\delta = 0.1$, $k = 0.2$, and $\mathrm{Nt} = 0.1$. To obtain illustrative results, Figures 2–4 are plotted to illustrate the impact of various involved parameters on the flow fields, thermal, and solutal distributions.

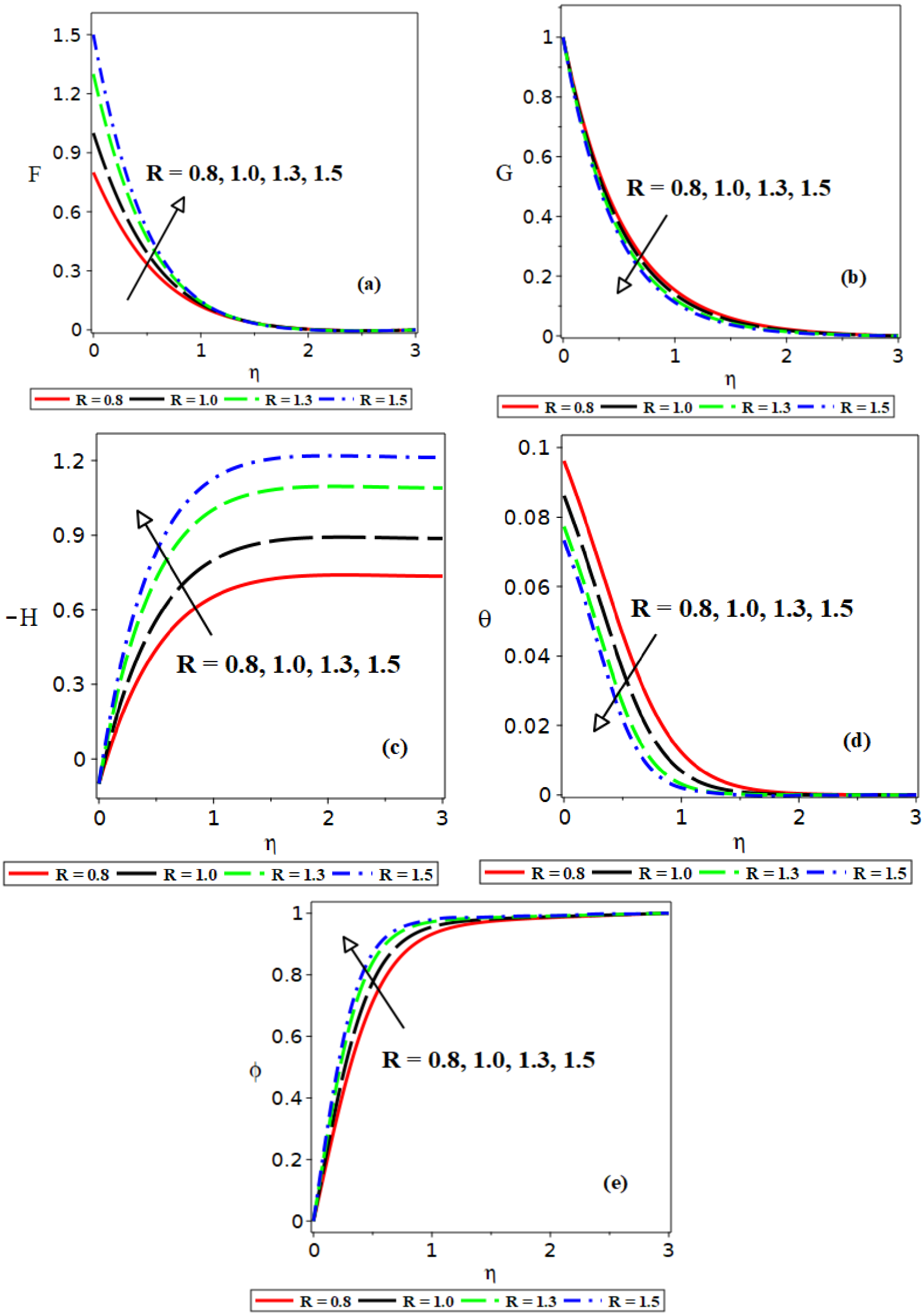

Figure 2. Effect of R on (**a**) F, (**b**) G, (**c**) $\{-H\}$, (**d**) θ, and (**e**) ϕ.

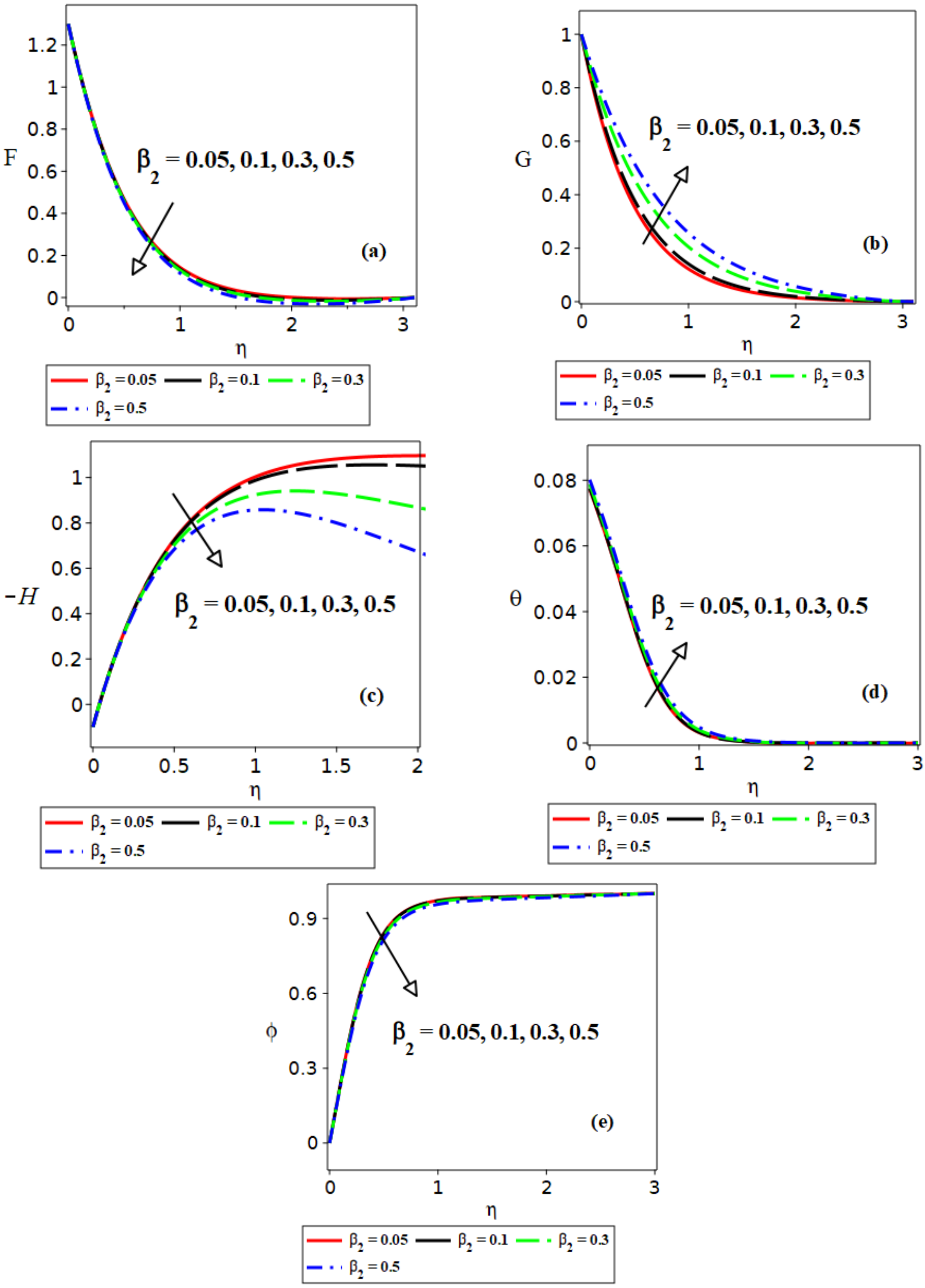

Figure 3. Effect of β_2 on (**a**) F, (**b**) G, (**c**) $\{-H\}$, (**d**) θ, and (**e**) ϕ.

Figure 2a–e highlight the effect of stretching parameter R on the flow, thermal, and solutal fields. The sketches make it clear that the velocity field is radially increasing and azimuthally decreasing. Because R is the stretch to swirl rate ratio, when the rate of the stretching parameter begins to thrive, the stretch rate becomes higher relative to the swirl rate. Therefore, the velocities enhance and reduce in the radial and angular directions, respectively. In addition, the axial velocity component shows a diminishing trend with an increasing rotating parameter, as shown in Figure 2c. Moreover, the evidence shown in Figure 2d indicates that the temperature of the fluid is decreasing as the stretching parameter becomes intensified. A converse trend can be seen for the mass concentration (see Figure 2e).

The influence of β_2 on the velocity, thermal, and solutal curves on a fixed magnetic parameter and stretching parameter, suction parameter, and porosity parameter are shown in Figure 3a–e. It is obvious that, as the relaxation time parameter, β_2, becomes powerful, the magnitude of the velocity curves decreases considerably in the radial and axial directions. In addition, an increase of β_2 from 0.05 to 0.5 has a positive effect on the angular velocity of the liquid. Moreover, curves are plotted in order to examine the impact that β_2 has on temperature as well as solutal distributions. It can be observed from the curves that the temperature of the liquid rises under the influence of β_2, while the mass concentration in the liquid reduces, as displayed in Figure 3d,e.

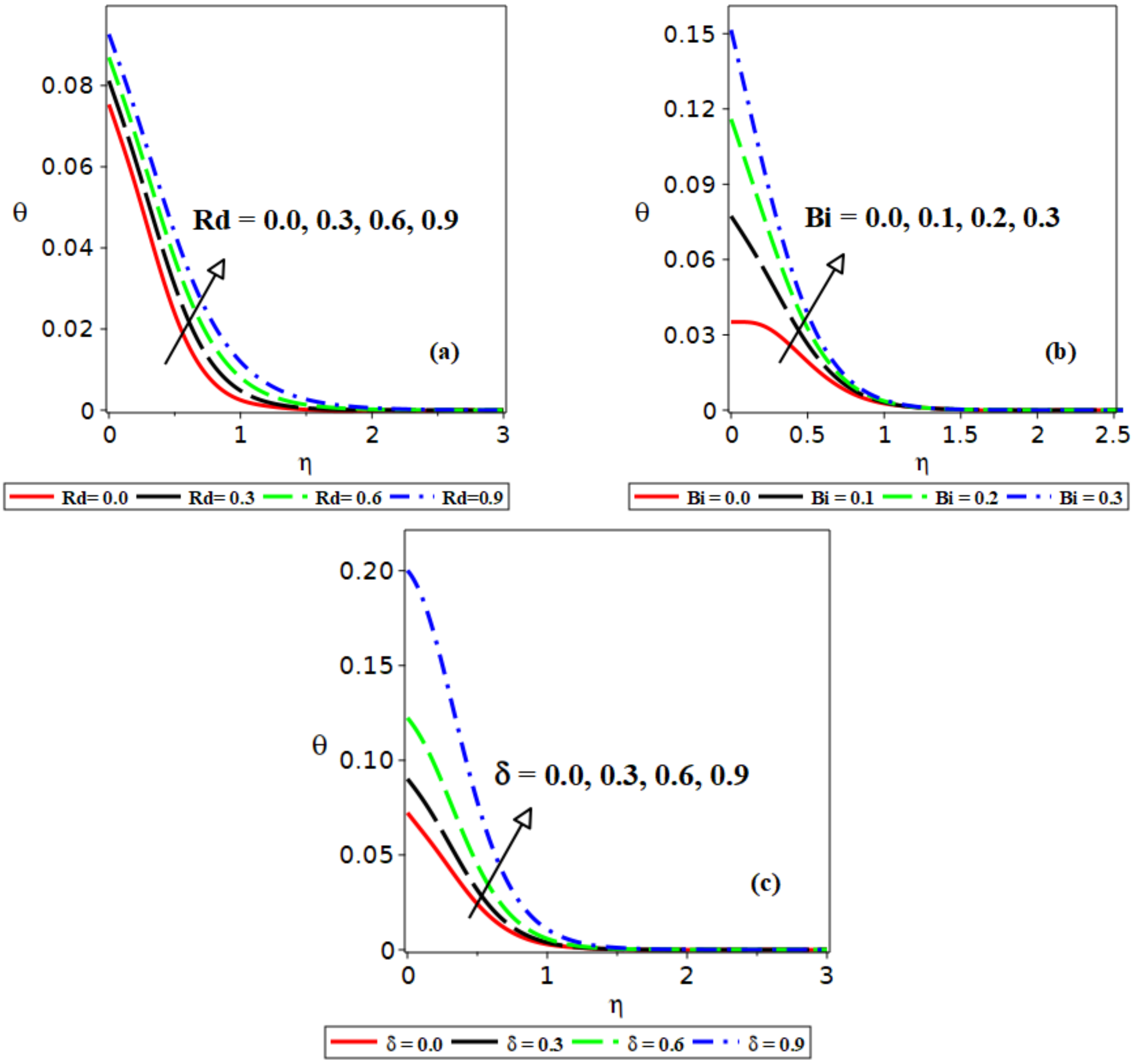

Figure 4. Variation of $\theta(\eta)$ on (**a**) Rd, (**b**) Bi, and (**c**) δ.

The elaboration of the curves of the thermal field for a variety of different values of Rd is shown in Figure 4a. The higher rate of Rd cause the thermal field to rise, along with the boundary layer thickness associated with it. As predicted, the presence of a radiation parameter, Rd, indicates that the fluid will absorb a greater amount of heat, which is equivalent to a higher temperature. Figure 4b indicates the peculiarities of the Biot number, Bi, on the fluid temperatures. In a physical point of view, an increase in the Biot number leads to larger convection at the disk surface, which in turn causes an increase in the fluid's temperature. In addition to this, the higher the Biot number, the more prominent the boundary layer thickness. A similar kind of trend may be seen on the thermal profile, which is caused by an increase in the heat generation parameter (see Figure 4c).

Table 1 displays the values of the local Nusselt number on β_1, β_2, Bi, Sr, and Du, respectively. The heat transfer rate increases with the increases in Bi and Sr, while it reduces due to the influence of β_1, β_2, and Du. The changes in mass transfer rate in the liquid due to Nt, K_r, k, Sr, and Du can be seen in Table 2. It is noted that the Sherwood number is a monotonically increasing function of Nt, k, and Du, while it is a decreasing function of K_r and Sr.

Table 1. Variation of $\mathrm{Re}^{-\frac{1}{2}}\mathrm{Nu_r}$ on β_1, β_2, Bi, Sr, and Du, respectively.

β_1	β_2	Bi	Sr	Du	$\mathrm{Re}^{-\frac{1}{2}}\mathrm{Nu_r}$
0.03	0.05	0.1	0.1	0.01	0.09229430
0.05					0.09227085
0.07					0.09224773
0.05	0.1				0.09224401
	0.2				0.09218679
	0.3				0.09212443
0.05	0.1	0.3			0.25443032
		0.5			0.39242589
		0.7			0.51127541
0.05	0.1	0.1	0.3		0.09229828
			0.5		0.09235327
			0.7		0.09241036
0.05	0.1			0.01	0.09224401
				0.05	0.07831140
				0.08	0.06707660

Table 2. Variation of $\mathrm{Re}^{-\frac{1}{2}}\mathrm{Sh_r}$ on Nt, K_r, k, Sr, and Du, respectively.

Nt	K_r	k	Sr	Du	$\mathrm{Re}^{-\frac{1}{2}}\mathrm{Sh_r}$
0.1	0.01	0.2	0.1	0.01	2.35092312
0.2					2.35418081
0.3					2.35767071
0.1	0.02				2.29027125
	0.03				2.23131286
	0.04				2.17416908
0.1	0.01	0.3			2.35253616
		0.4			2.35415123
		0.5			2.35596540
0.1	0.01	0.2	0.3		2.31108474
			0.5		2.26928009
			0.7		2.22710225

Table 2. *Cont.*

Nt	K_r	k	Sr	Du	$\mathbf{Re^{-\frac{1}{2}}Sh_r}$
0.1	0.01	0.2	0.1	0.02	2.34526541
				0.03	2.48338698
				0.05	2.63922405

Moreover, we computed $F'(0), -G'(0)$ and $-\theta'(0)$, and these results are compared with the available published results of [19,20] in Table 3, and it was found that they are in excellent agreement with each other.

Table 3. A link table between [19,20] with the current problem on fixed $\mathrm{Pr} = 6.5$ and $M = 0 = \gamma = R = s = \beta = \mathrm{Rd} = \delta = \mathrm{Du}$.

	[19]	[20]	Present Result
$F'(0)$	0.5102	0.51023262	0.5101162643
$-G'(0)$	0.6159	0.61592201	0.6158492796
$-\theta'(0)$	0.9337	0.93387794	0.9336941128

4. Conclusions

The axisymmetric swirling flow of Oldroyd-B fluid through a porous medium featuring the Soret–Dufour impacts is discussed. Further, heat and mass transportations are examined, along with numerous physical features. Numerical solutions are determined with the help of a numerical procedure. Below is a summary of some important findings:

- The magnitude of velocity curves decreases substantially in the radial and axial directions when the relaxation time parameter is changed to dynamic.
- A higher rate of radiation parameter causes the thermal field to rise, along with the boundary layer thickness associated with it.
- An increasing trend is observed on the thermal profile, which is due to the increase in the heat generation parameter.
- The higher the Biot number, the more pronounced is the thermal boundary layer thickness.
- The heat transfer rate enriches with an increase in the Soret number.
- The Sherwood number is a monotonically increasing function of the Dufour number.

Author Contributions: Conceptualization, A.K. and A.H.; methodology, A.A.E. and M.A.N.; software, A.H. and M.A.N.; validation, A.K. and A.A.E.; formal analysis, A.H.; investigation, A.H. and A.K.; resources, A.H.; data curation, A.H. and A.A.E.; writing—original draft preparation, A.H. and A.A.E.; writing—review and editing, A.K. and M.A.N.; visualization, A.A.E.; supervision, M.A.N.; project administration, A.H. and A.A.E.; funding acquisition, A.A.E. All authors have read and agreed to the published version of the manuscript.

Funding: This work was supported by the Deanship of Scientific Research, Vice Presidency for Graduate Studies and Scientific Research, King Faisal University, Saudi Arabia (Project No. GRANT 695).

Data Availability Statement: The data that support the findings of this study are available from the corresponding author upon reasonable request.

Acknowledgments: The authors would like to acknowledge the support from King Faisal University, Saudi Arabia (Project No. GRANT 695).

Conflicts of Interest: The authors declare no conflict of interest.

Nomenclature

r, φ, z	cylindrical coordinate	τ	heat capacities ratio
u, v, w	components of velocity	c_p	specific heat capacity
T	fluid temperature	T_∞	ambient temperature
T_f	convective fluid temperature	C_w	wall concentration
h_f	convective heat transfer coefficient	w_0	mass flux velocity
σ	the electric conductivity	μ	dynamic viscosity
ν	kinematic viscosity	ρ	fluid density
C	fluid concentration	C_∞	ambient concentration
D_m	molecular diffusion coefficient	K	permeability of medium
k_T	the thermal-diffusion ratio	K_1	the reaction rate
Ω	angular velocity rate	B_o	strength of magnetic field
c	stretching rate	c_s	the concentration susceptibility
λ_1	time relaxation	λ_2	time retardation
k	the thermophoretic coefficient	k^*	mean spectral absorption coefficient
M	magnetic field	k_1^*	thermal conductivity
σ^*	the Stefan-Boltzmann constant	β_1	relaxation time parameter
R	stretching parameter	γ	porosity parameter
β_2	retardation time parameter	Pr	Prandtl number
Bi	Biot number	K_r	the chemical reaction parameter
Re	the local Reynold number	Nt	relative temperature difference parameter
δ	heat source/sink	Rd	the radiation parameter
s	the suction parameter	Sc	Schmidt number
$\mathrm{Nu_r}$	the Nusselt number	$\mathrm{Sh_r}$	the Sherwood number
η	dimensionless variable	$'$	differentiation with respect to η
q_r	radiative heat flux	G	azimuthal velocity
H	axial velocity	F	radial velocity
θ	dimensionless temperature	ϕ	dimensionless concentration

References

1. Hafeez, A.; Khan, M.; Ahmed, J. Flow of magnetized Oldroyd-B nanofluid over a rotating disk. *Appl. Nanosci.* **2020**, *10*, 5135–5147. [CrossRef]
2. Kármán, T.V. Uber laminare and turbulente reibung. *Z. Angew. Math. Mech.* **1921**, *1*, 233–252. [CrossRef]
3. Cochran, W.G. The flow due to a rotating disk. In *Mathematical Proceedings of the Cambridge Philosophical Society*; Cambridge University Press: Cambridge, UK, 1934; Volume 30, pp. 365–375.
4. Millsaps, K.; Pohlhausen, K. Heat transfer by laminar flow from a rotating-plate. *J. Aeronaut. Sci.* **1952**, *19*, 120–126. [CrossRef]
5. Shevchuk, I.V.; Buschmann, M.H. Rotating disk heat transfer in a fluid swirling as a forced vortex. *Heat Mass Transf.* **2005**, *41*, 1112–1121. [CrossRef]
6. Awad, M.M. Heat transfer from a rotating disk to fluids for a wide range of Prandtl numbers using the asymptotic model. *J. Heat Transf.* **2008**, *130*, 014505. [CrossRef]
7. Turkyilmazoglu, M. Exact solutions corresponding to the viscous incompressible and conducting fluid flow due to a porous rotating disk. *J. Heat Transf.* **2009**, *131*, 091701. [CrossRef]
8. Turkyilmazoglu, M. Effects of uniform radial electric field on the MHD heat and fluid flow due to a rotating disk. *Int. J. Eng. Sci.* **2012**, *51*, 233–240. [CrossRef]
9. AL Nuwairan, M.; Hafeez, A.; Khalid, A.; Syed, A. Heat generation/absorption effects on radiative stagnation point flow of Maxwell nanofluid by a rotating disk influenced by activation energy. *Case Stud. Ther. Eng.* **2022**, *35*, 102047. [CrossRef]
10. Oldroyd, J.G. On the formulation of rheological equations of state. *Proc. R. Soc. Lond. Ser. A Math. Phys. Sci.* **1950**, *200*, 523–541.
11. Rajagopal, K.R.; Srinivasa, A.R. A thermodynamic frame work for rate type fluid models. *J. Non-Newtonian Fluid Mech.* **2000**, *88*, 207–227. [CrossRef]
12. Vieru, D.; Fetecau, C.; Fetecau, C. Flow of a generalized Oldroyd-B fluid due to a constantly accelerating plate. *Appl. Math. Comput.* **2008**, *201*, 834–842. [CrossRef]
13. Hafeez, A.; Khan, M.; Ahmed, J. Stagnation point flow of radiative Oldroyd-B nanofluid over a rotating disk. *Comput. Methods Programs Biomed.* **2020**, *199*, 105342. [CrossRef] [PubMed]
14. Lee, J.; Hwang, W.R.; Cho, K.S. Effect of stress diffusion on the Oldroyd-B fluid flow past a confined cylinder. *J. Non-Newtonian Fluid Mech.* **2021**, *297*, 104650. [CrossRef]
15. Shaqfeh, E.S.; Khomami, B. The Oldroyd-B fluid in elastic instabilities, turbulence and particle suspension. *J. Non-Newtonian Fluid Mech.* **2021**, *298*, 104672. [CrossRef]
16. Rosseland, S. *Astrophysik: Auf Atomtheoretischer Grundlage*; Springer: Berlin/Heidelberg, Germany, 1931; Volume 11, pp. 41–44.

17. Batchelor, G.K.; Shen, C. Thermophoretic deposition of particles in gas flowing over cold surfaces. *J. Colloid Interface Sci.* **1985**, *107*, 21–37. [CrossRef]
18. Talbot, L.; Cheng, R.K.; Schefer, R.W.; Willis, D.R. Thermophoresis of particles in a heated boundary layer. *J. Fluid Mech.* **1980**, *101*, 737–758. [CrossRef]
19. Bachok, N.; Ishak, A.; Pop, I. Flow and heat transfer over a rotating porous disk in a nanofluid. *Phys. B Condens. Matter* **2011**, *406*, 1767–1772. [CrossRef]
20. Turkyilmazoglu, M. Nanofluid flow and heat transfer due to a rotating disk. *Comput. Fluids* **2014**, *94*, 139–146. [CrossRef]